Light Metals 2015
Edited by: Margaret Hyland
TMS (The Minerals, Metals & Materials Society), 2015

HIGH-RATE FORMABILITY OF HIGH-STRENGTH ALUMINUM ALLOYS: A STUDY ON OBJECTIVITY OF MEASURED STRAIN AND STRAIN RATE

Piyush Upadhyay, Aashish Rohatgi, Elizabeth V. Stephens, Richard W. Davies, and David Catalini
Pacific Northwest National Laboratory, 902 Battelle Boulevard Richland, WA 99354, USA

Keywords: Digital Image Correlation, Formability, High Strain-Rate, Electro-hydraulic Forming

Abstract

Aluminum alloy AA7075 sheets were deformed at room temperature at strain-rates exceeding 1000 /s using the electrohydraulic forming (EHF) technique. A method that combines high speed imaging and digital image correlation technique, developed at Pacific Northwest National Laboratory, was used to investigate high strain rate deformation behavior of AA7075. For strain-rate sensitive materials, the ability to accurately model their high-rate deformation behavior is dependent upon the ability to accurately quantify the strain-rate that the material is subjected to. This work investigates the objectivity of software-calculated strain and strain rate by varying different parameters within commonly used commercially available digital image correlation software. The results show that except for very close to the time of crack opening the calculated strain and strain rates are consistent and independent of the adjustable parameters of the software.

Introduction

The Vehicle Technologies Office under the U.S. Department of Energy has set a goal of 50% reduction in weight of passenger-vehicle body and chassis system by 2015 compared to 2002 vehicle [1, 2]. To this end automotive manufacturers and stakeholders have identified the use of aluminum alloys as a viable light-weight replacement for steel in several automotive structural components. Aluminum alloys offer several advantages over steels including high strength to weight ratio, corrosion resistance and recyclability. One of the bottlenecks facing the industry in implementing aluminum sheet in automotive components is its poor formability characteristics at room temperature. Our research at the Pacific Northwest National Lab has been focused on developing methods to enhance room temperature formability by high-rate pulse-pressure forming. This work employs the electro-hydraulic forming (EHF) process which uses an intense pressure-pulse generated underwater by an electrical discharge to form sheet metals into single sided dies to produce a contoured shape. Formability enhancements in Al alloys have been observed and quantified when the strain-rates typically exceed 1000 /s [3, 4].

Traditionally considered to be weakly sensitive to strain-rate, aluminum alloys have been shown to exhibit strain rate sensitivity above certain strain-rates at room temperature [5–7]. For example, Figure 1 shows strain-rate sensitivity of flow stress at various temperatures in AA7075-T6 [8] and that this material shows a positive strain-rate sensitivity in the range of strain-rates tested. Similarly, Higashi et al [6] investigated flow stress of rolled AA5182 as a function of strain-rate ranging from 0.001 to 4000/sec. They showed that while at the strains of less than 5% the flow stress increased with increasing strain-rate (i.e. positive strain-rate sensitivity), the flow stress decreased with an increase in strain-rate between 0. 001/sec to 1000/sec (i.e. negative strain-rate sensitivity). Beyond strain-rate of ~1000/sec, the flow stress began to increase again at a significantly greater rate showing strong positive strain-rate sensitivity. These examples show that the constitutive behavior of aluminum alloys can be significantly impacted by the strain-rate during deformation. Hence developing the ability to accurately measure temporal strain and strain rate is critical to predict formability of aluminum alloys, particularly when the strain-rate during deformation spans several orders of magnitude, such as that occurs during EHF.

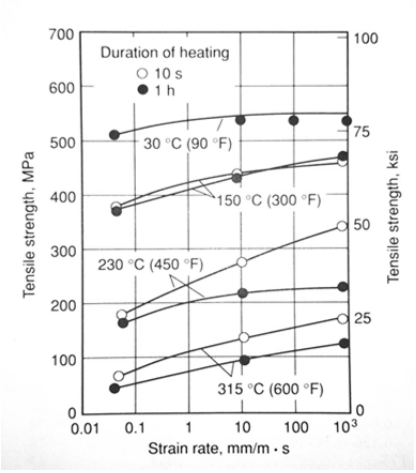

Figure 1. Flow stress vs. strain-rate in AA7075-T6 [8].

Over the years, digital image correlation (DIC) has been established as an effective non-contact / in-situ method to measure full-field surface displacements by tracking a random black and white speckle pattern. Commercially available software suites achieve this by comparing a reference image of the undeformed material with successive images of the deformed material, taken at known time intervals by one or more digital cameras. Each image is divided into a small square subset of a predefined size. A discrete matrix of pixel gray levels in each subset is used to identify unique points in subsequent images. Subset pixel gray levels are then correlated between the reference and deformed images to yield horizontal and vertical displacements. Finite Element shape functions are then used to calculate continuous displacement fields. Subsequently, velocities, strains, and strain-rates can be calculated for the full field using the measured surface displacements. Detailed descriptions of the DIC technique and its underlying theory can be found in [9–13].

Owing to its versatility, cost effectiveness and relative simplicity DIC technique is now being increasingly used in the research and development of automotive materials, especially in formability studies. However, there are no formal standards or guidelines to streamline the method of strain and strain-rate measurement using image correlation techniques. Lack of universally accepted standards leads to inevitable variations in image correlation approaches. Several factors might contribute to the variations including, but not limited to, the use of software packages from different vendors, version to version variations among the same software, user to user variation caused by selection of customizable parameters within the software like subset size, step size, filter size, and averaging algorithm to name a few.

Furthermore, verification of the temporal strain and strain-rate are intrinsically difficult. Conventionally, formability in deformed sheets is determined using the grid method. Although effective, the grid method can only provide final strain distribution while telling nothing about the strain path the material took to reach the final strain distribution. Experimental methods to verify strain-rates are also virtually nonexistent. A few reports of deformation history in high rate deformation are available but have only demonstrated limited success. Johnson et al. [14], for instance, reported using a laser-Doppler system to measure velocity vs. time data for electromagnetically expanding ring; however this was only possible for a few points and only along a single direction. Thus, researchers have mostly estimated the strain-rate by dividing the final strain value with the event duration. We have previously demonstrated a DIC-based novel technique to quantify full-field deformation history during high-strain-rate forming of aluminum alloys [3,15]. In this work we seek to examine the objectivity of the DIC-based procedures to calculate strain and especially strain-rate by changing various customizable parameters within the digital image correlation program.

Experimental Details

2.1 Electro-hydraulic forming setup and digital image correlation

1 mm thick AA7075-T6 sheets were free-formed using the EHF technique. A schematic of EHF and the high-speed image acquisition setup developed at PNNL is shown in Figure 2. The test specimen (Figure 3) discussed in this paper is termed as a single ligament or plane strain geometry. It consists of two symmetrical elliptical holes designed to provide a state of near-plane strain condition in the center of the sheet during forming. The cameras face the side of the specimen which was painted with a black and white speckled pattern for digital image correlation. The other side of the specimen was etched with a square grid pattern for conventional measurement of final strain. Right underneath the specimen a driver sheet (1 mm solid sheet of 5182-O without any holes) was placed. The contact surfaces of the test sheet and the driver sheet were coated with boron nitride lubricant to reduce contact friction. The driver sheet kept the water pressurized during the impact and prevented water from escaping the elliptical holes of the test sample. The discharge of the capacitor banks, charged to desired voltage, through a 0.3 mm diameter copper wire generated a pressure pulse in the water. This pressure pulse was responsible for deforming the sheet specimen into dome geometry via the driver sheet.

The sheet deformation process was captured by a pair of high speed Photron cameras at a rate of 75000 frames per second and a

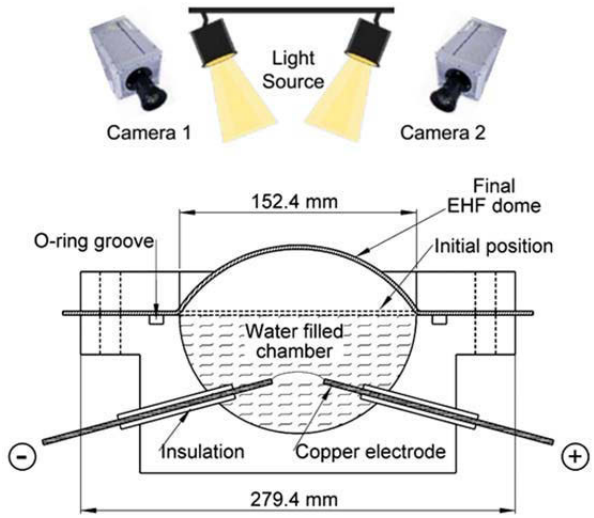

Figure 2. Schematic showing cross-section of EHF experimental setup with initial undeformed (dashed line) and final deformed position of test sheet.

resolution of 320 x 264 pixels, such that 1 pixel represented an area of approximately 0.6 mm × 0.6 mm. VIC 3D, version 2009.1.0. (Correlation Solutions Inc.), commercial DIC software, was then used to perform image correlation on a sequence of speckle pattern images to yield deformation history of the sheet. See [3,15] for additional details on test configuration and imaging setup. Post deformation strains near the crack locations were measured using automated image analysis software Automated Strain Analysis and Measurement Environment (ASAME, ASAME Inc.).

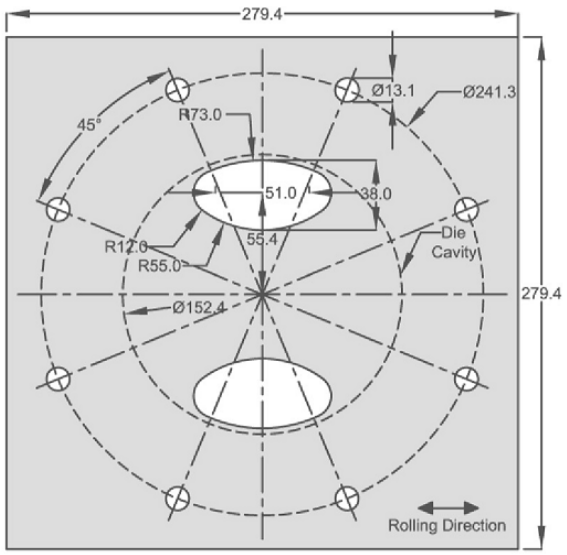

Figure 3. Schematic of specimen geometry tested. Two symmetric elliptical cutouts in the specimen provide a state of near-plane strain in the center of the sheet. The direction of major strain is along rolling direction.

Results and Discussions

Figure 4 shows the two halves of the test sample that fractured during the forming process. Because of significant deformation near the clamping region, the specimen has fractured away from the larger parent sheet. The strain and strain-rate maps obtained from DIC are shown in Figure 5. These maps correspond to the state of deformation ~13 microseconds prior to the crack initiation in the sample. The issue being addressed in this work is how these values change with changes in the software parameters. Although DIC-calculated strain values can be verified to some extent by comparing them with conventional strain grid measurements, no such direct verification exists for strain-rate, as discussed in the Introduction section. Even for the case of strain verification, this can only be made for the final strain value without knowing the strain path. In such situation it was deemed imperative to understand what effects various adjustable parameters within the VIC 3D software might have on the calculated strain and strain-rate fields.

In order to understand how the selected subset size may affect the software-calculated strain and strain-rate, a point near the crack region, identified in Figure 4 by a red dot, was chosen for temporal analysis. Strain and strain-rate values at this location for the duration of the forming process were calculated using three different subset sizes and various combinations of filter and step sizes. The subset size determines the size of the area of the speckle pattern being tracked between successive images. Step size on the other hand, determines the number of pixels between each subset. One such data set is presented in Figure 6 and Figure 7. In Figure 6 the strain values appear to be evolving in a similar manner in all the three cases resulting in almost identical strain values until the last time step after which the correlation is lost and no data point is available. The engineering strain for different subset sizes, for time step just prior to divergence is ~ 0.19. This value is close to the strain calculated from the strain grid of 0.23

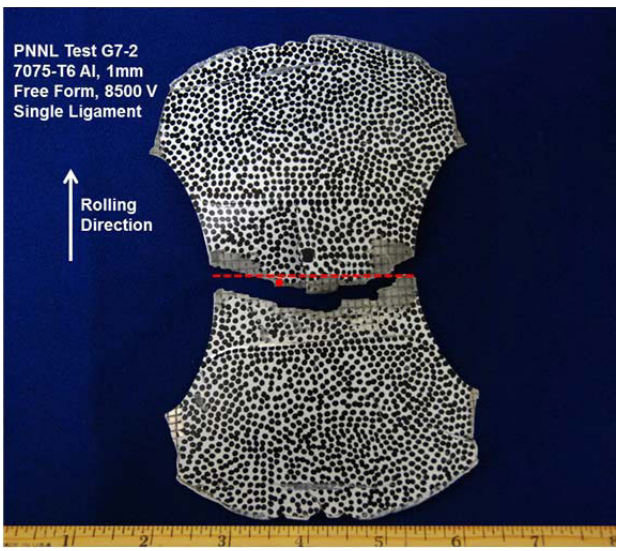

Figure 4. Post-formed plane-strain/single ligament specimen. The direction of major strain is along the rolling direction (the orientation is rotated 90º relative to that shown in Fig. 3). Note that the red dot and red broken line are indicative of location from where DIC strain and strain rate values were extracted *prior* to fracture.

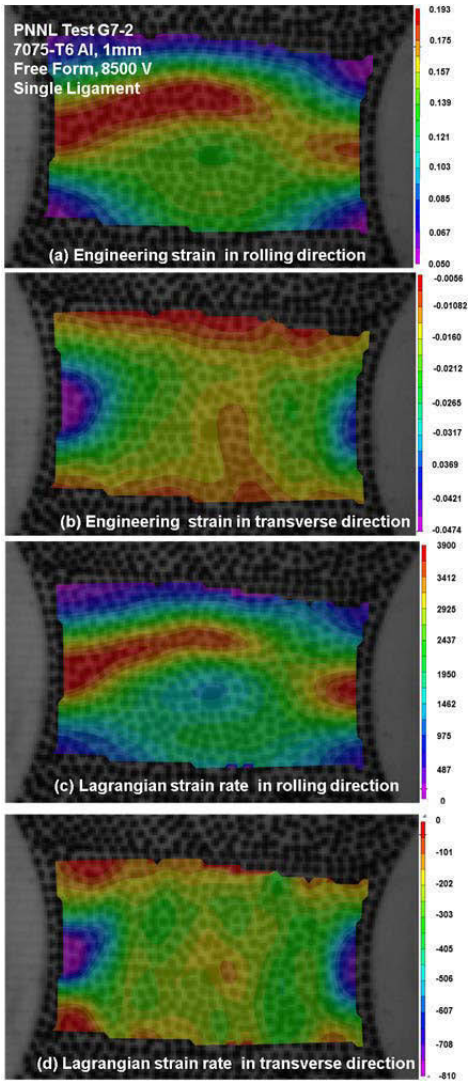

Figure 5. Color map of strain (a, b) and strain-rate (c, d) in two directions obtained from VIC 3D prior to fracture initiation. The rolling and transverse directions are oriented along the vertical and horizontal axes, respectively.

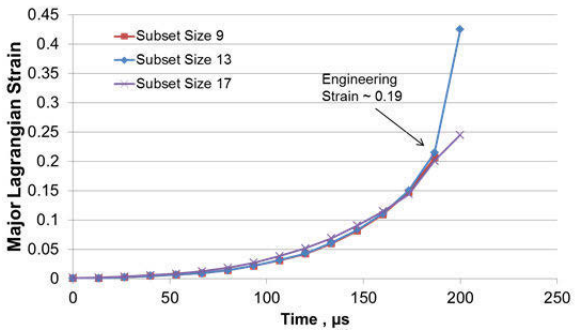

Figure 6. Major Lagrangian strain plotted against time for three different subset sizes. Filter size of 5 and step size of 1 was used.

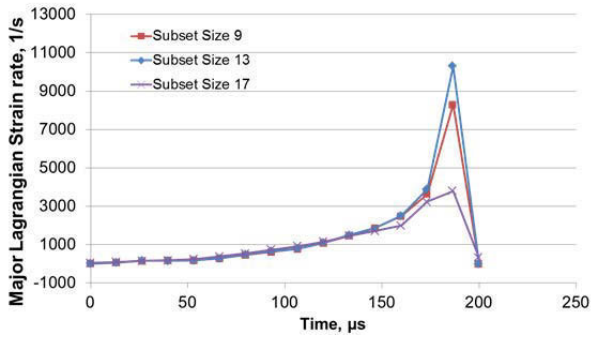

Figure 7. Major Lagrangian strain-rate plotted against time for three different subset sizes. Filter size of 5 and step size of 1 was used.

as shown in Figure 8 in the same vicinity. The strain-rate plot in Figure 7 also shows a similar trend as the strain plot in Figure 6. The DIC-calculated strain-rate is independent of the subset size except at the very end of the data when there is a sudden jump in strain-rate right before crack initiation. Since there is no direct method to verify which of these strain-rate values shown in Figure 7 are correct, this analysis suggests that strain-rate values towards the end of a data set need to be viewed with caution.

To further understand the strain and strain-rate variations with changes in DIC parameters, the strain /strain-rates across the transverse section of the samples (as seen by red dotted line in Figure 4) are examined. Two consecutive speckle images are considered - One image captured immediately prior to the

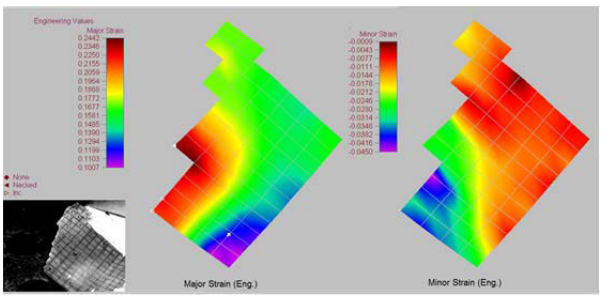

Figure 8. Color maps of major and minor engineering strains obtained from strain grid method.

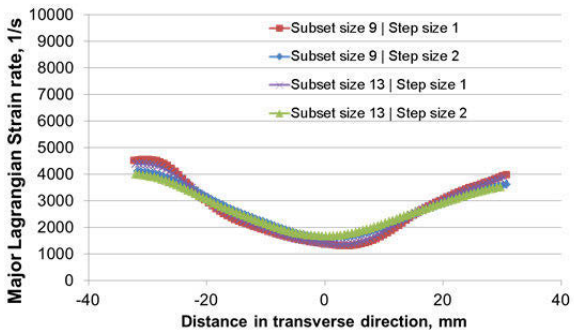

Figure 9. Strain-rate distribution across the sample for image $t_{crack-2}$ captured two frames prior to crack appearance in the sample.

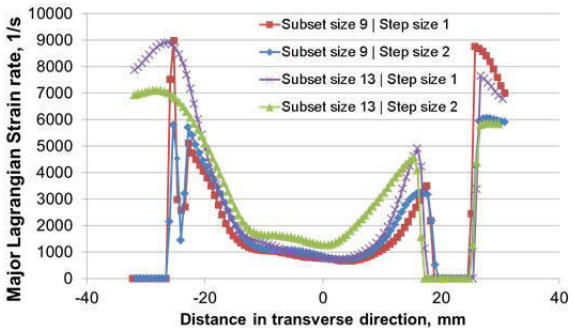

Figure 10. Strain-rate distribution across the sample for the image $t_{crack-1}$ captured two frames prior to crack appearance.

appearance of the crack in the specimen ($t_{crack-1}$) and another one captured two steps prior ($t_{crack-2}$). In this case the step size was also varied in addition to the subset size. Step size determines the spacing of each individual data points where displacement is calculated. As seen in Figure 9 for image $t_{crack-2}$, neither the step size nor the subset size has a significant effect on the strain-rate distributions across the sample. Similar trend, i.e. subset and step size independent strain-rate distribution, are obtained for all the images preceding $t_{crack-2}$. Figure 9 also shows that the strain-rates at the extremities of the sample are somewhat higher than those at the center, presumably because of the availability of free surface at the extremities (adjacent to the elliptical holes). In contrast to Figure 9, the data for the image $t_{crack-1}$ in Figure 10 shows that the choice of subset size and step size can affect the calculated strain-rate at time instances close to crack initiation. The difference in the strain-rate magnitude is especially magnified at the specimen edges. The data also shows that for the same subset size, the step size can also influence the magnitude of the calculated strain-rate.

Based on the above results, it appears that the calculated values of the strain-rate are most sensitive to software parameter when the data is analyzed near specimen edges and/or close to the instance of crack initiation. One reason for the above observations could be the delamination of the painted speckle pattern when approaching crack initiation. Since the DIC technique assumes

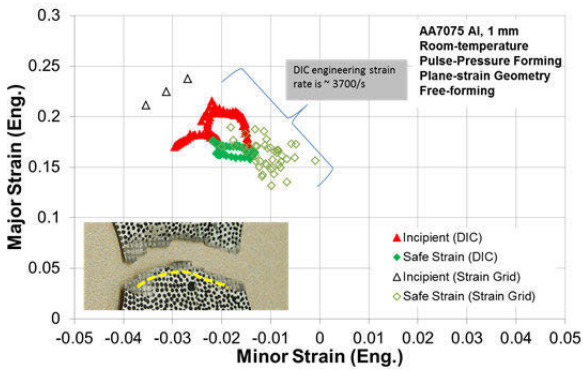

Figure 11. Comparison between strain calculated from DIC (Subset size 9, Step size 1, and Filter size 5) and that obtained from grid method. The approximate locations in the sample from where DIC safe strains were extracted are shown by yellow dotted lines in the inset.

that sheet deformation is manifested as the deformation of the speckle pattern, any loss of adhesion between the paint and the test sheet will lead to erroneous values. However such loss of adhesion is difficult to identify positively from the raw images.

Finally, Figure 11 compares the strains obtained from the DIC technique (Subset size 9, Step size 1, and Filter size 5) and those obtained via conventional grid measurement method. The incipient strain locations were visually identified from fractured specimens and strains away from the incipient locations were deemed to be safe. Considering that the strain grid method can have an error of up to 2% strain, Fig. 11 shows that the DIC-calculated strain values are in good agreement with the values obtained from the conventional strain grid method in the same vicinity. One possible way to identify the correct software parameters is to ensure that the DIC-calculated strain matches that determined by the strain grid method. One may also vary the subset size, step size etc. until their calculated strain-rate converges to similar values. Nevertheless, the results show that when examining DIC data away from specimen edges and prior to crack initiation, the calculated strain-rate and strain values can be used with confidence.

Conclusion

A method combining high speed imaging and digital image correlation technique was used to investigate high-strain-rate deformation behavior of Al 7075-T6. The effects of various parameters in the DIC software were studied to ascertain robustness of the calculated strain and strain-rate history. Based on the data analyzed, the following conclusions can be drawn:

1) Except for very close to the time of crack initiation and near the specimen edges, the strain-rate calculated by DIC is effectively independent of the parameter selected.
2) The in-situ DIC-calculated strain value is in good agreement with the post-mortem strain measured by the conventional strain grid method.
3) The DIC technique has been successfully implemented to quantify the high-rate forming behavior of Al alloys

Acknowledgements

The Pacific Northwest National Laboratory is operated by Battelle Memorial Institute for the U.S. Department of Energy under contract DE-AC05-76RL01830. This work was sponsored by W. Joost in association with the U.S. Department of Energy, Office of Vehicle Technologies, as part of the Lightweight Materials program. The authors would like to thank the U.S. automotive industry partners for their suggestions in the course of this work. Technical support by J. Johnson (Bonneville Power Administration), A. Tofts and H. Schreier (Correlated Solutions), and PNNL staff M.T. Smith, G.L. Vanarsdale, M.E. Dahl, and K.F. Mattlin, is gratefully acknowledged.

References

[1] "President Announces New Fuel Economy Standards | The White House" [Online]. Available: http://www.whitehouse.gov/blog/2011/07/29/president-obama-announces-new-fuel-economy-standards.

[2] 2012 DOE Vehicle Technologies Office Annual Merit Review.

[3] Rohatgi, A., Stephens, E. V., Soulami, A., Davies, R. W., and Smith, M. T., 2011, "Experimental characterization of sheet metal deformation during electro-hydraulic forming," Journal of Materials Processing Technology, **211**(11), pp. 1824–1833.

[4] Rohatgi, A., Soulami, A., Stephens, E. V., Davies, R. W., and Smith, M. T., 2014, "An investigation of enhanced formability in AA5182-O Al during high-rate free-forming at room-temperature: Quantification of deformation history," Journal of Materials Processing Technology, **214**(3), pp. 722–732.

[5] Higashi, K., Mukai, T., Kaizu, K., Tsuchida, S., and Tanimura, S., 1991, "Strain rate dependence on mechanical properties in some commercial aluminum alloys," Le Journal de Physique IV, Colloque C3, Vol. 1, pp. C3–341–C3–346.

[6] Higashi, K., Mukai, T., Kaizu, K., Tsuchida, S., and Tanimura, S., 1991, "The microstructural evolution during deformation under several strain rates in a commercial 5182 aluminium alloy," Le Journal de Physique IV, Colloque C3, Vol. 1, pp. C3–347–C3–352.

[7] Smerd, R., Winkler, S., Salisbury, C., Worswick, M., Lloyd, D., and Finn, M., 2005, "High strain rate tensile testing of automotive aluminum alloy sheet," International Journal of Impact Engineering, **32**(1–4), pp. 541–560.

[8] Davis, J. R., 1993, Aluminum and Aluminum Alloys, ASM International, pp 697.

[9] Sutton, M., Wolters, W., Peters, W., Ranson, W., and McNeill, S., 1983, "Determination of displacements using an improved digital correlation method," Image and Vision Computing, **1**(3), pp. 133–139.

[10] Lyons, J. S., Liu, J., and Sutton, M. A., 1996, "High-temperature deformation measurements using digital-image correlation," Experimental Mechanics, **36**(1), pp. 64–70.

[11] Pan, B., Qian, K., Xie, H., and Asundi, A., 2009, "Two-dimensional digital image correlation for in-plane displacement and strain measurement: a review," Meas. Sci. Technol., **20**(6), p. 062001.

[12] Sutton, M. A., Orteu, J. J., and Schreier, H., 2009, Image Correlation for Shape, Motion and Deformation Measurements: Basic Concepts,Theory and Applications, Springer Science & Business Media.

[13] Wang, K., Carsley, J. E., He, B., Li, J., and Zhang, L., 2014, "Measuring forming limit strains with digital image correlation analysis," Journal of Materials Processing Technology, **214**(5), pp. 1120–1130.

[14] Johnson, J. R., Taber, G., Vivek, A., Zhang, Y., Golowin, S., Banik, K., Fenton, G. K., and Daehn, G. S., 2009, "Coupling Experiment and Simulation in Electromagnetic Forming Using Photon Doppler Velocimetry," Steel Research International, **80**(5), pp. 359–365.

[15] Aashish Rohatgi, Ayoub Soulami, Elizabeth V. Stephens, Richard W. Davies, and Mark T. Smith, 2014, "An investigation of enhanced formability in AA5182-O Al during high-rate free-forming at room-temperature: Quantification of deformation history," Journal of Materials Processing Technology, **214**(3), pp. 722–732.